Sensors and Materials, Vol. 31, No. 2 (2019) 509–518
MYU Tokyo

S & M 1791

Multi-input Multi-output Magnetoelectric Dipole Antennas Comprising Dual Monopole Feed Antennas for Energy Harvesting

Wen-Shan Chen, Chien-Min Cheng,* and Guang-Ren Zhang

Department of Electronic Engineering, Southern Taiwan University of Science and Technology
No. 1, Nan-Tai Street, Yungkang Dist., Tainan City 710, Taiwan R.O.C.

(Received June 12, 2018; accepted October 22, 2018)

Keywords: multi-input multi-output, energy harvesting, magnetoelectric dipole antenna, electromagnetic band gap

A three-dimensional (3-D) inverted-L multi-input multi-output (MIMO) magnetoelectric dipole antenna comprising two coupled monopole feed antennas is developed for energy-harvesting applications. Additionally, the electromagnetic band-gap (EBG) structure was used to improve the isolation (S_{21}) of the antennas. The bandwidth of the proposed antenna is up to 42.1% for 3–4.6 GHz, which covers the C-band (5G) applications of 3.3–3.8 GHz. The advantages of the proposed antenna are the following: low cross-polarization; good radiation patterns; stable and high gains (9.55 ± 0.35 dBi) in the operating band; all simulated and measured return loss of the antennas (S_{11} and S_{22}) are below −10 dB; and the isolation between two antennas is below −15 dB. Finally, the proposed antenna is suitable for modern energy-harvesting and 5G wireless sensor network systems.

1. Introduction

With the continuous innovation of Internet of Things (IoT) technology and requirement of sensors, for low loss and low environmental pollution of modern electronic products, antennas are used to harvest the free electromagnetic energy in the surroundings, and then, it is converted to electric energy through radio-frequency (RF) circuits. To harvest more electromagnetic energy and from greater distances, antennas with high gains have been developed by many researchers. In 2006, Luk and Wong presented a novel magnetoelectric dipole antenna with a wideband, low cross-polarization, low backlobe, and stable radiation patterns. A three-dimensional (3-D) inverted-L dipole antenna was designed and fed by a quarter-wavelength ($\lambda/4$) inverted-L probe. As the probe is excited, it will generate a magnetic dipole that combines with the electric dipole generated by the antenna; hence, its impedance bandwidth can be increased effectively.(1) For a simple feed method and better antenna efficiency, the differential feed technique using two symmetric structures was developed for the 3-D inverted-L dipole antenna. The advantages of this feed technique are an increase in the impedance bandwidth, decrease in cross-polarization, and decrease in the backlobe.(2) The reflection phase of the artificial

*Corresponding author: e-mail: ccmin523@gmail.com
https://doi.org/10.18494/SAM.2019.2107

ISSN 0914-4935
https://myukk.org/

magnetic conductor (AMC) is 0 and can be put under the loop antenna to decrease the height and increase the gains of the antenna.[3] For the Yagi antenna, the gains for GSM-1800 (1.805–1.88 GHz) and UMTS-2100 (2.11–2.17 GHz) are 10.9 and 13.3 dBi, respectively. The energy transform efficiency is as high as 40%, enabling the use of the Yagi antenna in electric energy harvesting.[4] The rectenna has a simple structure, high gain of 8.6 dBi, maximum energy transform efficiency of 83% (operated at 2.45 GHz), and minimum energy transform efficiency of 50% even though the input power is only 17.2 dBm, making it applicable to energy harvesting.[5] The transform efficiency of energy harvesting could be increased by using high-gain antennas with rectified circuits, solar panels, or folded antennas.[6–9] A wideband dipole rectenna with a vertical metal plate was used to reduce the backlobe to 8.4 dB, which enables an increase in its energy transform efficiency.[10] A differentially fed microstrip antenna with a high gain of 8.5 dBi, high efficiency of 80%, and operated at GSM-900 (900–960 MHz) was presented. It could be applied at the front of the RF circuits and modified the impedance matching for efficiency improvement.[11]

To find the best antenna for energy harvesting, the short dipole antenna, patch antenna, and Yagi antenna were compared. It was found that a small antenna could not satisfy the requirements of energy harvesting, but the combination of a Yagi antenna and rectifier yielded much better results than other antennas.[12] In this work, to obtain better antenna efficiencies, gains, and a faster transmission speed of signals, we developed a 3-D inverted-L multi-input multi-output (MIMO) magnetoelectric dipole antenna. On the basis of the idea of the hinge antenna of notebook computers, the feed technique of this proposed antenna was to use two coupled monopole antennas to excite the closed slots located between two hinges.[13,14] These two coupled monopole feed antennas excited the slots and generated the magnetic dipole, which combines with the electric dipole generated by the inverted-L dipole antenna. Two similar beam widths can be obtained for *YZ* and *XZ* planes, and they can cover the modern C-band (5G) of 3.3−3.8 GHz. Furthermore, we also used the electromagnetic band-gap (EBG) structure to suppress the surface current occurring between two antennas, and finally increased its isolation and reduced the interference to enable energy-harvesting applications.[15–17]

2. Antenna Design

2.1 Antenna structure

A 3-D MIMO magnetoelectric dipole antenna was designed and fabricated on a flame retardant 4 (FR4) substrate with a thickness of 0.8 mm, permittivity (ε_r) of 4.4, and loss tangent (tanδ) of 0.0245. The proposed antenna was composed of an 85 × 85 mm^2 metal reflector, four polyactide (PLA) pillars, a 42 × 17 mm^2 metal ground, an EBG structure, two coupled monopole feed antennas, and a pair of 3-D inverted-L dipole antennas, as Fig. 1 shows. Additionally, four PLA pillars were added between the ground and the reflector. They were made using a 3-D printer and had a height of 15 mm, tan δ of 0.25, and ε_r of 4. Two inverted-L dipole antennas were excited by two coupled monopole antennas resonated at 3.65 GHz with an electric length of half the guided wavelength (λ/2). However, on both sides of the metal ground,

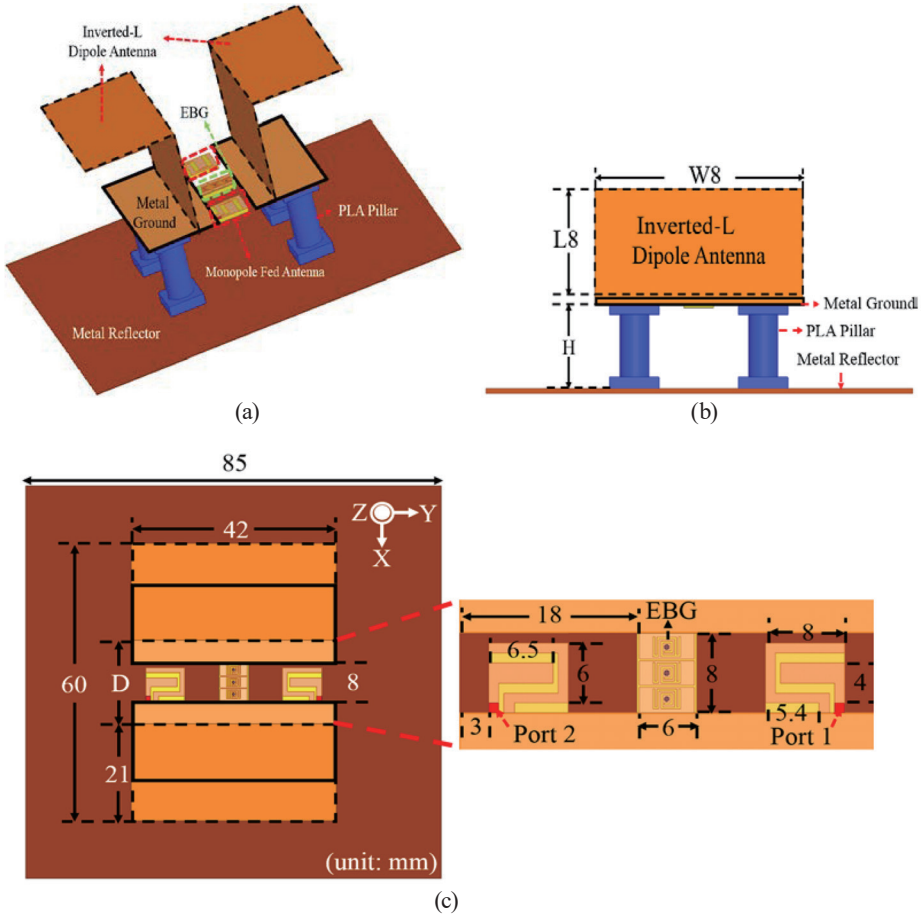

Fig. 1. (Color online) Geometry of proposed antenna: (a) 3-D, (b) side view, and (c) top view.

two open slots were also excited by these two feed antennas, generating a magnetic dipole that resonated at 4.1 GHz with an electric length of one-quarter the guided wavelength ($\lambda/4$) and that combined with the electric dipole generated by the inverted-L dipole antennas. Two similar and stable beamwidths can thus be generated with low cross-polarization for both *YZ* and *XZ* planes. In the previous paper,[18] the authors expanded the applications of the photonic crystals to the microwave field because of its band-gap property, and designed some equivalent circuit structures for generating a band-gap effect of specified frequency. Thus, it was called the EBG structure. As shown in Fig. 2(a), the mushroom-like EBG proposed by Sievenpiper *et al.* is the most widely studied and discussed. It is an array composed of square metal sheets that are connected to the ground plane through a via located at the center of each metal sheet. This structure will generate capacitive effects owing to the electric field existing among the metal sheets, and the current flow through the via will generate inductive effects owing to the magnetic field. These two effects are equivalent to a parallel LC circuit.[19]

In this work, to increase the amount of coupling and generate a band gap at about 2.7 GHz, we used FR4 as the substrate and developed a modified EBG structure with three groups of

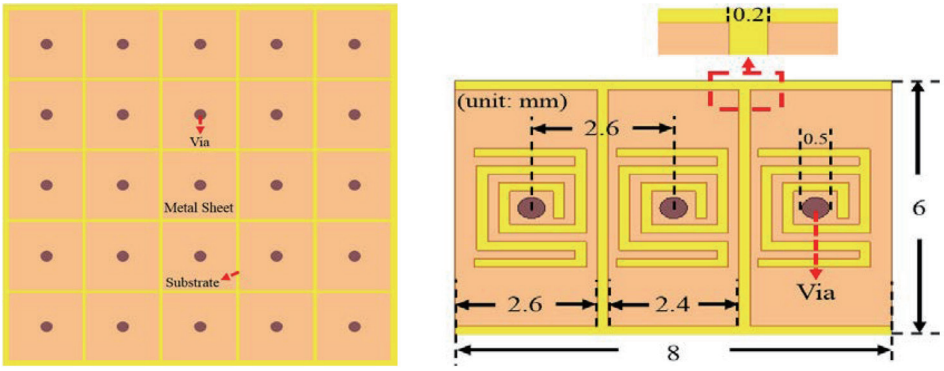

(a) (b)

Fig. 2. (Color online) Geometry of EBGs: (a) mushroom-like EBG[18] and (b) dual-spiral EBG (proposed).

compact dual spirals and vias, as shown in the center of Fig. 1(c) and enlarged in Fig. 2(b). The EBD structure was composed of three dual spirals and connected to the back metal plane through three vias with copper rods. However, two metal grounds are connected by the EBG and thus two open slots existed between them. These slots can increase the equivalent capacitance and the spiral structure can increase the equivalent inductance.[20,21]

2.2 Suspending microstrip line measurement of proposed EBG

To investigate the isolation influences of the EBG between these two coupled monopole antennas, we adopted the suspended microstrip line measurement to analyze the EBG. In addition, the EBG was sandwiched tightly between two FR4 substrates and connected to the back metal plane through the via, as shown in Fig. 3. Then the microstrip line was fabricated on the upper FR4 substrate and connected to two SubMiniature version A (SMA) connectors. The strong mutual coupling effect between the microstrip line and EBG reduces the parasitic effects generated by other devices, and hence, reveals the band-gap properties.[20,21] The simplified equivalent parallel LC circuit is shown in Fig. 4 and its resonant frequency (f_s) can be derived as Eq. (1), where L is the inductance due to current flows through the via, C_1 is the capacitance between the upper microstrip line and the EBG, and C_2 is the capacitance between the EBG and the back metal ground. It can be seen that the increasing capacitance or inductance will cause the decrease in resonant frequency. Additionally, the three dual spirals also generate parts of inductance and capacitance for C_1, C_2, and L. The measured and simulated isolation (S_{21}) for 2–5 GHz are plotted in Fig. 5. It is found that the EBG reveals better-simulated S_{21} (lower than −20 dB) at about 2.7 GHz. However, the measured S_{21} shifts to lower frequency and reveals better impedance matching and bandwidth, which is consistent with previous reports.[22,23] Figure 6 shows the S_{21} values with and without (with metal sheet) the EBG. It is seen that without the EBG, the influence between two antennas is serious (greater than −15 dB) for 3.3–4.7 GHz. However, after EBG is used, the resonant frequency of the EBG is shifted

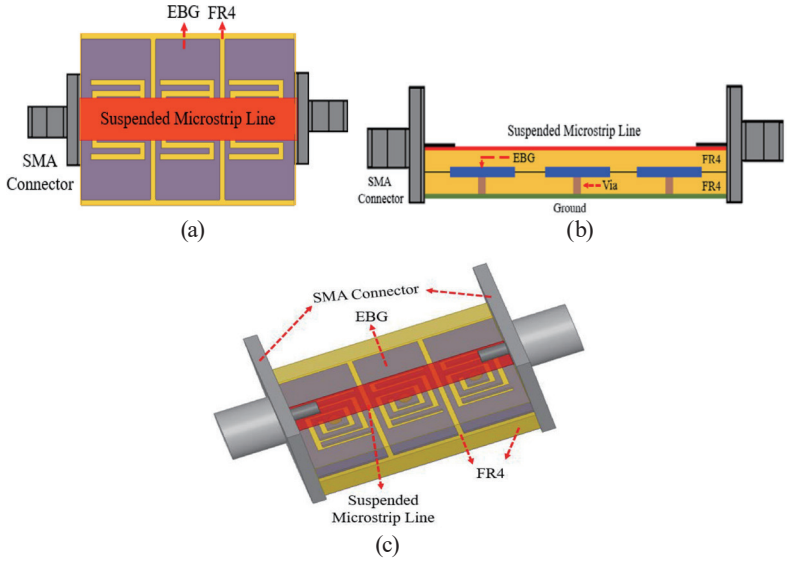

Fig. 3. (Color online) Suspended microstrip line measurement of EBG: (a) top view, (b) side view, and (c) 3-D view.

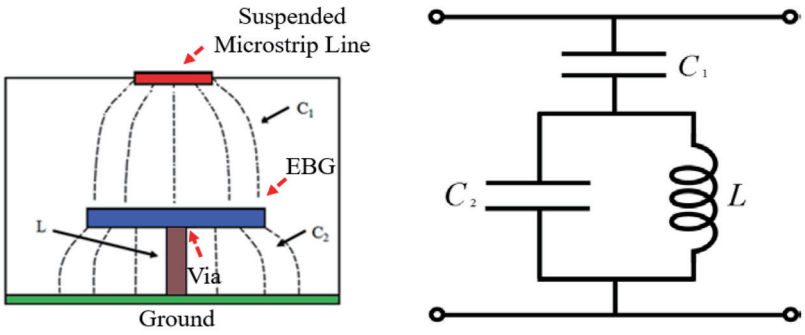

Fig. 4. (Color online) Simplified equivalent circuit of EBG.

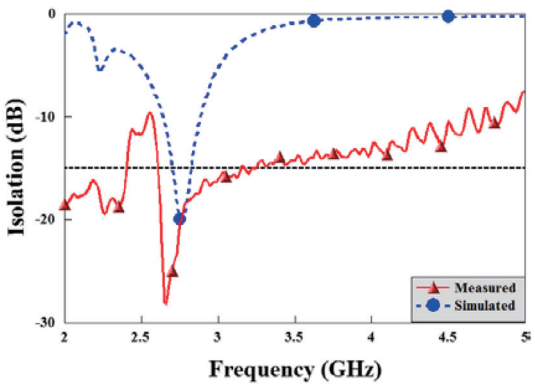

Fig. 5. (Color online) Simulated and measured S parameters of EBG for suspended microstrip line measurement.

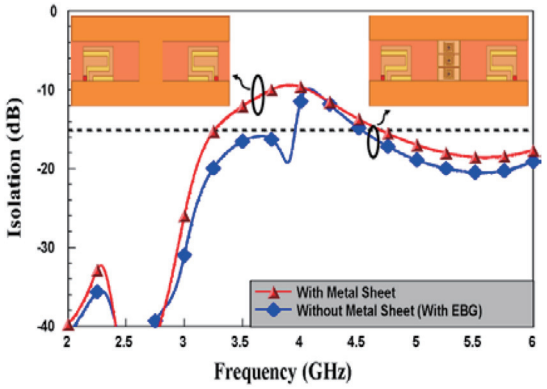

Fig. 6. (Color online) Simulated S_{21} values with and without metal sheet (with EBG).

from 2.7 to 3.8 GHz, which means that the isolation is modified and better than that without the EBG. Figure 7 shows the current distribution plots in the case of with and without the EBG. Compared with without the EBG, we find that the surface current is obviously suppressed by the use of the EBG and hence, the isolation is improved.

$$f_s = \frac{1}{2\pi\sqrt{L(C_1+C_2)}} \tag{1}$$

3. Results and Discussion

Figure 8 shows the simulated S parameters for different distances between two inverted-L dipole antennas (D values) with the PLA pillar height (H) fixed at 15 mm. From the simulated S_{11} and S_{22} curves shown in Fig. 8(a), with D values equal to 14–18 mm, all the S parameters are below −10 dB for 3.3–4.4 GHz. This means that the excitation wavelengths of two coupling feed antennas will decrease owing to the increase in the distance between two inverted-L dipole antennas. In addition, the first resonated mode (at about 3.65 GHz) and the second resonated mode (at about 4.1 GHz) are all shifted to higher frequencies as D values are decreased. Figure 8(b) shows S_{21}, and we can see that as D values are decreased, the two inverted-L antennas will

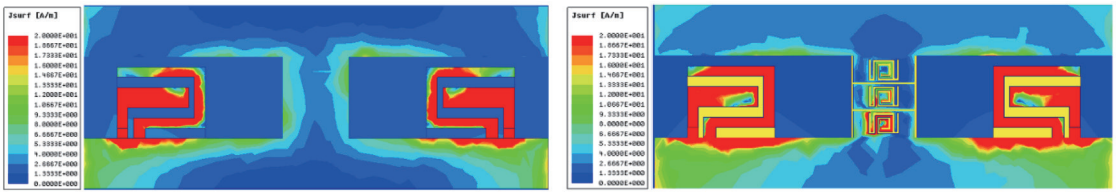

(a) (b)

Fig. 7. (Color online) Simulated 3.8 GHz current distribution plots: (a) with metal sheet and (b) without metal sheet but with EBG.

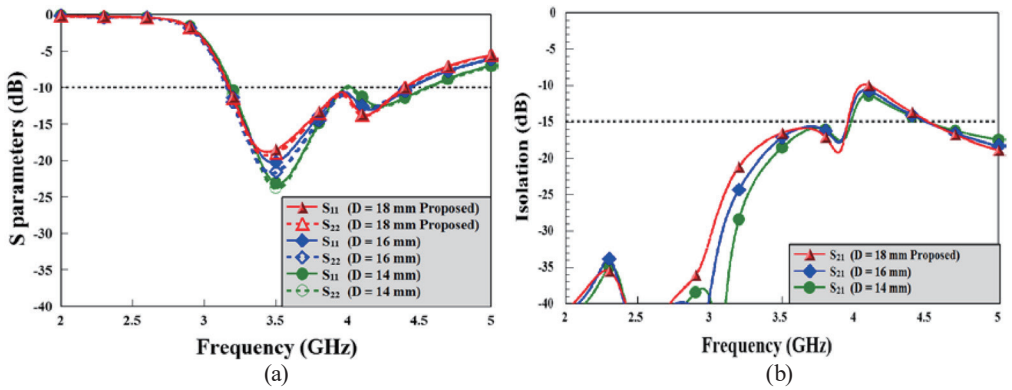

(a) (b)

Fig. 8. (Color online) Simulated S parameters for different D values (H = 15 mm): (a) S_{11} and S_{22} and (b) S_{21}.

become closer to the two feed antennas. Thus, the isolation will gradually worsen. Figure 9 shows the simulated antenna gains for different D values (H is fixed at 15 mm). It can be seen that for the operation band (3.3–3.8 GHz), the antenna gains clearly decrease with decreasing D values. This phenomenon is caused by the variation of the radiation patterns, which is induced by the alterations of the electric and magnetic dipoles. Additionally, as the D value is 18 mm, we can obtain high antenna gains easily and with the maximum gain of 10.4 dBi (at 3.5 GHz) and the minimum gain of 9.9 dBi (at 3.8 GHz).

For the distance between two inverted-L dipole antennas fixed at 18 mm, Fig. 10 shows the simulated return loss for different H values (13, 14, and 15 mm). We find, from the simulated return loss shown in Fig. 10(a), that all the S_{11} and S_{22} values are below −10 dB for 3.3–4.4 GHz. This means that all resonated modes of the antenna were affected by the air thickness and the heights of the PLA pillars. Furthermore, we can see from the S_{21} plots shown in Fig. 10(b) that, as H values decrease, the metal reflector will become closer to the metal ground, and

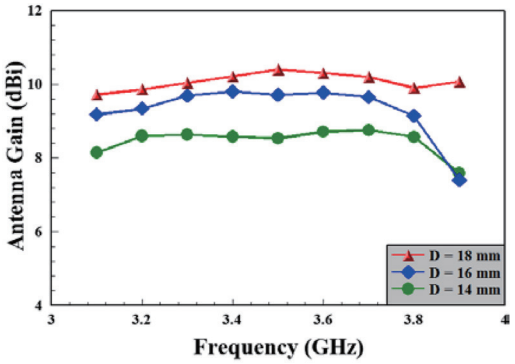

Fig. 9. (Color online) Simulated antenna gains for different D values (H = 15 mm).

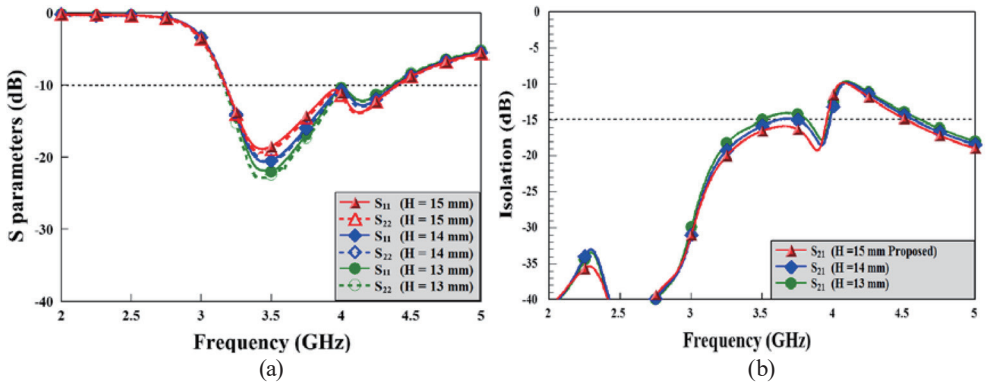

Fig. 10. (Color online) Simulated S parameters for different H values (D = 18 mm): (a) S_{11} and S_{22} and (b) S_{21}.

thus the isolation will gradually worsen (greater than −15 dB at H = 14 mm). Figure 11 shows the simulated antenna gains for different H values (D is fixed at 18 mm). It can be seen that for the operation band of 3.3–3.8 GHz, the antenna gains decrease with decreasing H. This phenomenon may be caused by the variation in the impedance matching owing to different H values. Additionally, when the H value is 15 mm, the maximum gain is 10.4 dBi (at 3.5 GHz) and the minimum gain is 9.9 dBi (at 3.8 GHz).

For H of 15 mm and D of 21 mm, the simulated and measured S parameters (S_{11}, S_{22}, and S_{21}) of the proposed antenna are shown in Fig. 12. It is found that for the operation band of 3.3–3.8 GHz, both the simulated and measured return losses (S_{11} and S_{22}) are lower than −10 dB. In addition, all the measured S_{21} values are lower than −15 dB. Compared with the simulated impedance bandwidth of 32.5% (3.17–4.4 GHz), the measured impedance bandwidth (3–4.6 GHz) increased by about 9.6% to 42.1%. Owing to fabrication errors and the use of the EBG, the resonant frequency shifted to a lower frequency but was still within the range of C-band (5G) applications of 3.3–3.8 GHz. Figure 13 shows the simulated and measured 2-D *YZ*- and *XZ*-plane radiation patterns of the proposed antenna for 3.3, 3.4, 3.5, and 3.6 GHz. We find, from the figure, that both the simulated and measured radiation patterns reveal similar beamwidths in both the *YZ* and *XZ* planes. This means that this proposed antenna achieves stable and unidirectional radiation patterns and lower cross-polarization.

Figure 14 shows the simulated and measured antenna gains and efficiencies. In the operation band of 3.3–3.8 GHz, on comparing these two figures, we can see that both the simulated results are more stable than the measured one. For the simulated results shown in Fig. 14(a), the gain is stable with a variation of only 4.9%. The minimum value is 9.9 dBi at 3.2 GHz and the maximum value is 10.4 dBi at 3.5 GHz. Moreover, the lowest simulated efficiency is 80% at 3.8 GHz, and the highest simulated efficiency is 91% at 3.3 GHz. However, for the measured results shown in Fig. 14(b), the gain is stable with a variation of 7.3%, a minimum value of 9.2 dBi at 3.2 GHz, and a maximum value of 9.9 dBi at 3.5 GHz. Moreover, the lowest measured efficiency is 61% at 3.8 GHz, and the highest measured efficiency is 75.8% at 3.3 GHz.

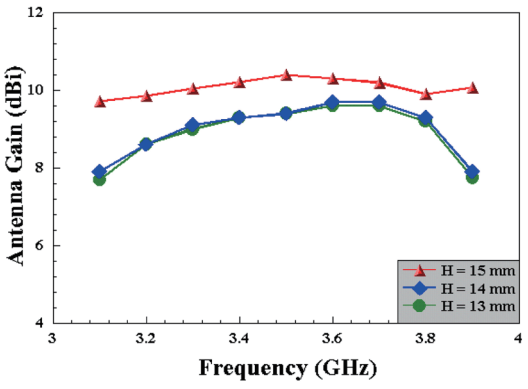

Fig. 11. (Color online) Simulated antenna gains for different H values (D = 18 mm).

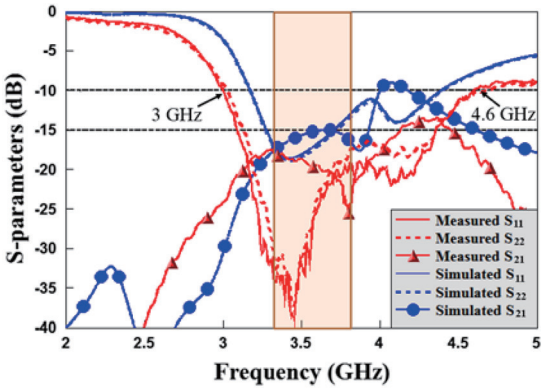

Fig. 12. (Color online) Simulated and measured S parameters (H = 15 mm, D = 21 mm).

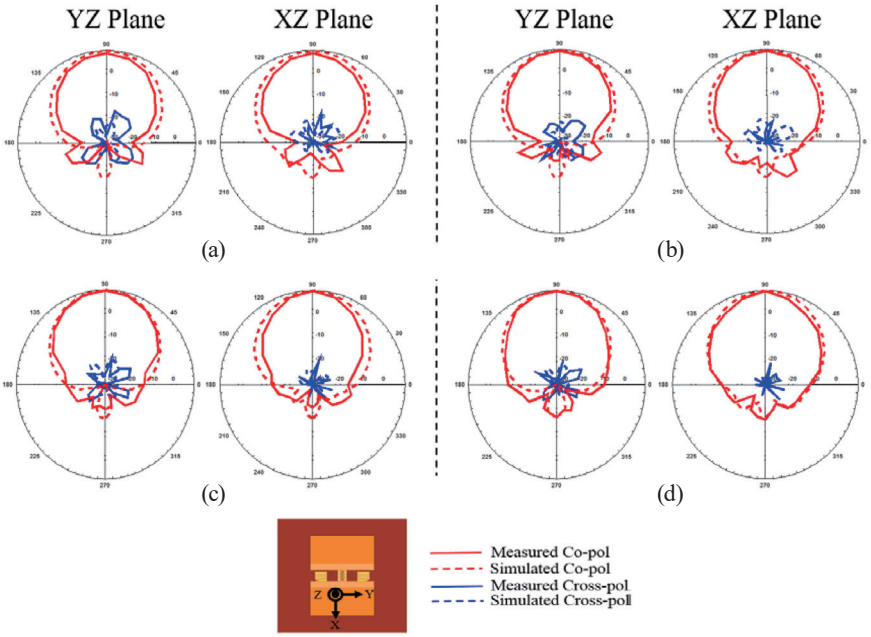

Fig. 13. (Color online) Simulated and measured antenna radiation patterns: (a) 3.3, (b) 3.4, (c) 3.5, and (d) 3.6 GHz.

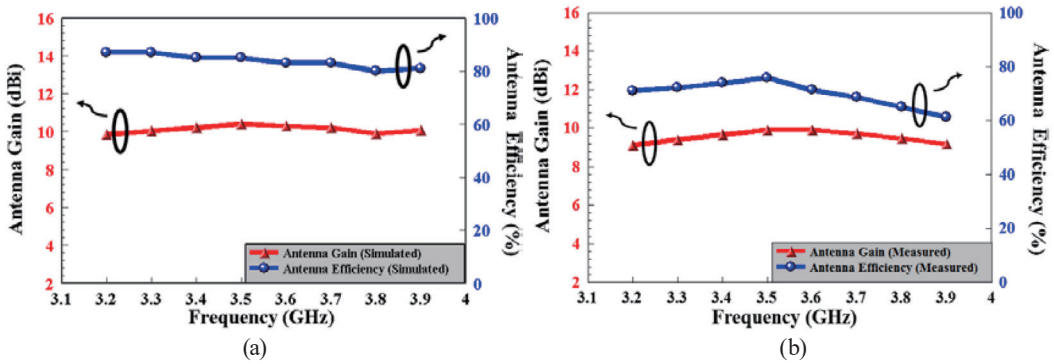

Fig. 14. (Color online) (a) Simulated and (b) measured antenna gains and efficiencies.

Table 1
Simulated and measured characteristics (H = 15 mm, D = 18 mm).

Bands (GHz)		Max. gain (dBi)	Min. gain (dBi)	Max. efficiency (%)	Min. efficiency (%)	Gain variation (%)
3.3–3.8	Simulated	10.4	9.9	90	80	4.9
	Measured	9.9	9.2	75.8	61	7.3

4. Conclusions

With two coupling monopole antennas for excitation and the addition of a metal reflector, a 3-D inverted-L MIMO magnetoelectric dipole antenna with stable radiation patterns and high antenna gains and efficiencies was achieved. The EBG structure was used to suppress the surface current between two dipole antennas and hence increase their isolation. As shown in Table 1, for the C-band (5G) applications of 3.3–3.8 GHz, with H = 15 mm and D = 18 mm, the optimum properties of the proposed antenna were high stability (simulated variation was 4.9% and measured variation was 7.3%), high antenna gains (simulated: 10.4 dBi; measured: 9.9 dBi), high efficiency (simulated: 90%; measured: 75.8%), low cross-polarization, return loss below −10 dB, and isolations below −15 dB. The proposed antenna is thus suitable for future energy-harvesting applications and 5G wireless sensor network systems.

Acknowledgments

This work was kindly supported by the Ministry of Science and Technology of the Republic of China (MOST 106-2221-E-218-034).

References

1 K. M. Luk and H. Wong: Int. J. Microwave Opt. Technol. **1** (2006) 34.
2 S. W. Liao, Q. Xue, and J. H. Xu: IEEE Antennas Propag. Mag. **55** (2013) 74.
3 H. Kamoda, S. Kitazawa, N. Kukutsu, and K. Kobayashi: IEEE Trans. Antennas Propag. **63** (2015) 4408.
4 H. C. Sun, Y. X. Guo, M. He, and Z. Zhong: IEEE Antennas Wirel. Propag. Lett. **12** (2013) 918.
5 H. C. Sun, Y. X. Guo, M. He, and Z. Zhong: IEEE Antennas Wirel. Propag. Lett. **11** (2012) 929.
6 Y. Tawk, J. Costantine, F. Ayoub, and C. G. Christodoulou: IEEE Antennas Propag. Mag. **60** (2018) 132.
7 S. Karimkashi and A. A. Kishk: IEEE Trans. Antennas Propag. **57** (2009) 3813.
8 F. Xie, G. M. Yang, and W. Geyi: IEEE Antennas Wirel. Propag. Lett. **12** (2013) 155.
9 T. S. Almoneef, H. Sun, and O. M. Ramahi: IEEE Antennas Wirel. Propag. Lett. **15** (2016) 1406.
10 J. I. Moon, I. K. Cho, S. M. Kimand, and Y. B. Jung: Electron. Lett. **49** (2013) 1050.
11 M. Arrawatia, M. S. Baghini, and G. Kumar: IEEE Trans. Antennas Propag. **63** (2015) 1983.
12 P. Soboll, V. Wienstroer, and R. Kronberger: IEEE Microwave Mag. **17** (2016) 75.
13 S. C. Chen and Y. C. Tsou: IEEE Trans. Antennas Propag. **52** (2016) 794.
14 S. C. Chen and Y. C. Tsou: IEEE Trans. Antennas Propag. **64** (2016) 3707.
15 S. D. Assimonis, T. V. Yioultsis, and C. S. Antonopoulos: IEEE Trans. Magn. **48** (2012) 771.
16 G. E. Domínguez, J. M. F. Gonzalez, P. Padilla, and M. S. Castañer: IEEE Antennas Wirel. Propag. Lett. **11** (2012) 1265.
17 S. D. Assimonis, T. V. Yioultsis, and C. S. Antonopoulos: IEEE Trans. Antennas Propag. **60** (2012) 4944.
18 E. Yablonovitch: J. Opt. Soc. Am. **10** (1993) 283.
19 D. Sievenpiper, L. Zhang, R. F. Jimenez Broas, N. G. Alexopolous, and E. Yablonovitch: IEEE Trans. Microwave Theory Tech. **47** (1999) 2059.
20 L. Yang, M. Fan, and Z. Feng: Asia-Pacific Microwave Conf. (APMC) (2005) 4.
21 L. H. Mei, Z. Hua, S. S. Ming, and F. S. Wei: 4th Asia-Pacific Conf. Anten. Propag. (APCAP) (2015) 307.
22 S. Y. Wang and F. C. Chen: 42nd Eur. Microwave Conf. (EuMC) (2012) 663.
23 Z. Yan, Z. Ning-ning, S. Q. Lin, L. S. Wei, and Z. Jun: Int. Conf. Meas. Tech. Mech. Auto. (ICMTMA) (2011) 350.